Aalborg Universitet

AALBORG UNIVERSITY

Investigation of Operating Range of Marine Growth Removing ROV under Offshore Disturbances

von Benzon, Malte; Liniger, Jesper; Sørensen, Fredrik Fogh; Pedersen, Simon

Investigation of Operating Range of Marine Growth Removing ROV under Offshore Disturbances

Malte von Benzon [**], **Jesper Liniger**, **Fredrik Fogh Sørensen**,
Simon Pedersen,

AAU Energy, Aalborg University, Niels Bohrs Vej 8, DK-6700 Esbjerg,
Denmark
** *Corresponding author. E-mail: msrvb@energy.aau.dk).*

Abstract: Marine growth on offshore underwater structures is a problem as it reduces the lifespan. The structures are cleaned annually by manually operated ROVs. Automation of these ROVs can improve the removal efficiency, and thereby reduce the cleaning campaign time and cost, as it is challenging for the operators to manually stabilize the ROVs under the harsh offshore conditions. Waves, ocean currents, the attached tether and the cleaning tool all generate external forces to the ROVs acting as substantial disturbances which can be rejected by a controller. This study examines the operating range of a standard compact ROV subject to external disturbances. To analyze the cleaning performance a normalized performance parameter is defined which weight the relative distance of the water jet with the most efficient distance. The results show that the waves has a larger effect on the cleaning performance compared to the ocean current. This paper examines the operating range of a reconfigured BlueROV2. For Hs$\leq$ 1.4 m it is possible to clean in the entire operating range. To clean at all the considered sea states Hs$\leq$ 3m and ocean currents of 0.1 - 0.5 ms^{-1} the ROV needs to be below 13 m.

Keywords: ROV, Underwater Robotics, Offshore, Irregular Waves, Tether Dynamics, Disturbance Rejection, SMC

1. INTRODUCTION

Offshore underwater structures are subject to a layer of marine growth, both hard(mussels and barnacles) and soft(algae) growth, which in average increases the hydrodynamic loads by 17.5% and the weight by 0.15% (Yan and Yan (2003)), which consequently increases the material fatigue and lowering the lifespan of the structures; Pedersen et al. (2022). Today, manual operated ROVs are used to remove marine growth from offshore structures usually using high pressure water jetting, however, automation of the ROVs can reduce the cost of operation for the offshore industry; Energy Supply (2020); Tena (2011); Energy Research (2020). In Benzon et al. (2021), a control algorithm based on a modified sliding model controller (SMC) was proposed and experimentally tested to automate an ROV to withstand the force from the high pressure water jet in a cleaning scenario performed in an onshore test facility. However, autonomous operation with ROVs near offshore structures also demands a controller which is able to reject disturbances from, water waves, the communication/power tether, ocean currents and the interaction between them these forces. This will be the investigation of this paper.

The contribution of this paper is an investigation of the operation range in an offshore environment for near-structure autonomous operations for a marine growth removing ROV. The results will be obtained based on simulations with an experimentally validated model of a reconfigured BlueROV2 and the environmental-induced forces acting as disturbances. The BlueROV2 is chosen due to the availability of a verified model and it being fully controllable Benzon et al. (2021). The results will highlight which operating conditions, consisting of wave height, depth and underwater ocean current, the ROV can efficiently tolerate in a marine growth removal campaign. The controller used in this investigation is derived and experimental validated in Benzon et al. (2021) on the same setup in an onshore non-disturbed environment. A description of near structure operation is presented in section 2, a mathematical model of the ROV in section 3, and a full disturbance model in section 4. The controller will be introduced in section 6 and the results will be presented in section 7. Lastly a conclusion and future work will be presented.

2. NEAR STRUCTURE OFFSHORE OPERATION CONDITIONS

The operational conditions in an offshore environment is highly disturbed by water waves, the communication tether, ocean current and the interaction between them. This makes operating with free floating ROVs challenging especially when the operation is close to offshore structures and requires small errors, such as for marine growth cleaning; Pedersen et al. (2022). In addition to the environmental disturbances there is also a disturbance from the high pressure water jet. This investigation will be based in the North Sea, where the statistical parameters used in this

study to model the disturbances is gathered. The median significant wave height is 1-2 meter with a wave period of 6.1 seconds. This investigation will consider sea states up to 3-4 meter significant waves height, the investigated sea states are shown in Table 1. The current at these sea states can be up to 0.5 ms^{-1}, and will be evaluated at 0.1, 0.3 and 0.5 ms^{-1}. The direction of the waves and current will be from north-west which is the most likely direction. The ROV cleaning trajectory will start at 30 meter depth. The trajectory stops at 5 meter below mean sea level(MSL). The cleaning velocity will be 0.06 ms^{-1}.

Table 1. Wave and current constants

Significant wave height H_s(m)	Period T_p(sec)
3.0	7.75
2.8	7.58
2.6	7.39
2.4	7.20
2.2	6.98
2.0	6.75
1.8	6.50
1.6	6.23
1.4	5.97
1.2	5.70
1.0	5.38
0.8	4.97
0.6	4.40
0.4	3.84
0.2	3.39

It is assumed that the tether of the ROV is fixed above sea level. The water hose will be ignored in this investigation, as it is assumed that the water hose will be wrapped with the tether.

3. ROV MODELING

The mathematical model of the ROV is based on Fossen's representation for marine vehicles Fossen (2011), and the parameters have been determined through a combination of experiments and CAD models. The model of the ROV is described further in Benzon et al. (2021) where the same platform has been used. The governing equations are given by.

$$\dot{\boldsymbol{\eta}} = \boldsymbol{J}(\boldsymbol{\eta})\boldsymbol{\nu} \qquad (1)$$

$$\boldsymbol{M}\dot{\boldsymbol{\nu}} + \boldsymbol{C}(\boldsymbol{\nu})\boldsymbol{\nu} + \boldsymbol{D}(\boldsymbol{\nu})\boldsymbol{\nu} + \boldsymbol{g}(\boldsymbol{\eta}) = \boldsymbol{\tau} + \boldsymbol{\tau_j} + \boldsymbol{\tau_t} + \boldsymbol{\tau_w} \quad (2)$$

where $\boldsymbol{\eta} = [N, E, D, \phi, \theta, \psi]^T$ is a combination of world coordinates and Euler angles defined in the NED frame. $\boldsymbol{\nu} = [u, v, w, p, q, r]^T$ is the body-fixed velocity vector. $J(\eta)$ is the rotation matrix. $\boldsymbol{\tau_j}$, $\boldsymbol{\tau_t}$ and $\boldsymbol{\tau_w}$ is the external disturbance force from the water jet, the tether and the waves respectively. The other variables are shown in Table 2 with parameters in Table 3. In Fig. 1 both the NED and body-fixed frame definitions are shown.
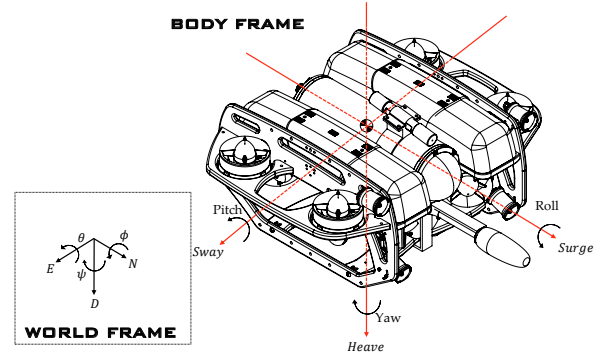

Fig. 1. Figure from Benzon et al. (2021). Reconfigured BlueROV2 with frame-definitions in both body and world frame, respectively.

Table 2. Variables and their components

Notation	Components
$\boldsymbol{M}$	$\boldsymbol{M}_{RB} + \boldsymbol{M}_A$
$\boldsymbol{M}_{RB}$	$\text{diag}(m, m, m, I_x, I_y, I_z)$
$\boldsymbol{M}_A$	$-\text{diag}(X_{\dot{u}}, Y_{\dot{v}}, Z_{\dot{w}}, K_{\dot{p}}, M_{\dot{q}}, N_{\dot{r}})$
$\boldsymbol{C}(\boldsymbol{\nu})$	$\begin{bmatrix} \boldsymbol{0} & \boldsymbol{C}_1(\boldsymbol{\nu}) \\ \boldsymbol{C}_1(\boldsymbol{\nu}) & \boldsymbol{C}_2(\boldsymbol{\nu}) \end{bmatrix}$
$\boldsymbol{C}_1(\boldsymbol{\nu})$	$\begin{bmatrix} 0 & (m - Z_{\dot{w}})w & (Y_{\dot{v}} - m)v \\ (Z_{\dot{w}} - m)w & 0 & (m - X_{\dot{u}})u \\ (m - Y_{\dot{v}})v & (X_{\dot{u}} - m)u & 0 \end{bmatrix}$
$\boldsymbol{C}_2(\boldsymbol{\nu})$	$\begin{bmatrix} 0 & -(I_z + N_{\dot{r}})r & (M_{\dot{q}} - I_y)q \\ (N_{\dot{r}} + I_z)r & 0 & (I_x - K_{\dot{p}})p \\ (I_y - M_{\dot{q}})q & (K_{\dot{p}} - I_x)p & 0 \end{bmatrix}$
$\boldsymbol{D}(\boldsymbol{\nu})$	$-\text{diag}(X_u(u), Y_v(v), Z_w(w), K_p(p), M_q(q), N_r(r))$
$\boldsymbol{g}(\boldsymbol{\eta})$	$\begin{bmatrix} (W - B)\sin(\theta) \\ -(W - B)\cos(\theta)\sin(\phi) \\ -(W - B)\cos(\theta)\cos(\phi) \\ y_b B\cos(\theta)\cos(\phi) - z_b B\cos(\theta)\sin(\phi) \\ -z_b B\sin(\theta) - x_b B\cos(\theta)\cos(\phi) \\ x_b B\cos(\theta)\sin(\phi) + y_b B\sin(\theta) \end{bmatrix}$
W	mg
B	$\rho g \nabla$
$\boldsymbol{\tau}$	$[\tau_1, \tau_2, \tau_3, \tau_4, \tau_5, \tau_6]^T$

Table 3. Parameters used for the model.

Notation	Values/Term	Unit
g	9.82	m s^{-2}
ρ	1000	kg m^{-3}
m	13.5	kg
∇	0.0133	m^3
(I_x, I_y, I_z)	(0.26, 0.23, 0.37)	kg m^2
(x_b, y_b, z_b)	(0, 0, -0.01)	m
$X_{\dot{u}}$	6.36	kg
$Y_{\dot{v}}$	7.12	kg
$Z_{\dot{w}}$	18.68	kg
$K_{\dot{p}}$	0.189	kg m^2
$M_{\dot{q}}$	0.135	kg m^2
$N_{\dot{r}}$	0.222	kg m^2
$X_u(u)$	$141|u| + 13.7$	N s m^{-1}
$Y_v(v)$	$184.3|v| + 20$	N s m^{-1}
$Z_w(w)$	$190|w| + 33$	N s m^{-1}
$K_p(p)$	$0.95|p| + 0.15$	N s
$M_q(q)$	$0.47|q| + 0.8$	N s
$N_r(r)$	$1.17|r| + 0.2$	N s

4. MODELING OF EXTERNAL DISTURBANCES

In this section, we will briefly outline how the external disturbances are found.

4.1 Water jet

The force from the water jet is modelled as a constant force, since the ROV will be cleaning, hence the water will be on. The constant force is found from momentum analysis to be -16.6 N in the forward direction relative to the body frame Benzon et al. (2021), with a flow of 0.01 $m^3 s^{-1}$ at 100 MPa pressure.

$$\boldsymbol{\tau_j} = [-16.6, 0, 0, 0, 0, 0]^T \tag{3}$$

4.2 Ocean waves

Table 4. Definitions of variables

Notation	Description
a	Wave amplitude
c	Spreading index
d	Water depth
f	Wave frequency
f_P	Peak wave frequency
H_s	The significant wave height
L	Wavelength
i, j	Index number
k	Wavenumber
n and m	Natural numbers
$S(f, \zeta), S_{JS}(f)$	Water wave spectrum
T_p	Peak wave period
t	Time
$X(\zeta)$	Spreading function
γ	Peak enhancement factor
ζ	Wave direction
Π	Surface elevation
Θ	Angular wave frequency
$\Gamma(n)$	Gamma function
μ	Random phase

The disturbance due to wave motion is taken into account by a relative Morison-type equation Avila and Adamowski (2011); Sayer (2008); DNV (Det Norske Veritas) (2021) expressed here as

$$\boldsymbol{\tau}_w = \boldsymbol{D}_w \left(\boldsymbol{\nu}_w - \boldsymbol{\nu}_1\right) |\boldsymbol{\nu}_w - \boldsymbol{\nu}_1| + \left(\boldsymbol{M}_w \dot{\boldsymbol{\nu}}_w - \boldsymbol{M}_{a,w} \dot{\boldsymbol{\nu}}_1\right) \tag{4}$$

where $\boldsymbol{\nu}_w = (u_w, v_w, w_w)$ is the particle velocity of the fluid, and $\boldsymbol{D}_w (\boldsymbol{\nu}_w - \boldsymbol{\nu}_1) = \boldsymbol{D}(1{:}3, 1{:}3)$ is the drag force, $\boldsymbol{M_w} = \boldsymbol{M}(1{:}3, 1{:}3)$. $\boldsymbol{M}_{a,w} = \boldsymbol{M_a}(1{:}3, 1{:}3)$ is the added mass and $\boldsymbol{\nu_1} = [u, v, w]^T$ is the fluid particle velocity. The fluid particle velocity is computed based on the JONSWAP wave spectrum Hasselmann (1973) including a spreading function that allows for short-crested sea states, i.e. multi-directional and irregular water waves,

$$S(f, \zeta) = S_{JS}(f) X(\zeta) \tag{5}$$

The JONSWAP spectrum can be expressed as,

$$S_{JS}(f) = C(\gamma) \frac{5}{16} H_s^2 \frac{f_P^4}{f^5} e^{\left(-\frac{5 f_P^4}{4 f^4}\right)} \gamma^{e^{\left(-\frac{(f - f_P)^2}{2(\sigma f_P)^2}\right)}} \tag{6}$$

where $C(\gamma) = 1 - \ln(\gamma) 0.287$ is a normalizing factor, γ is the peak enhancement factor, H_s is the significant wave height, $f_p = \frac{1}{T_p}$ is the peak frequency, T_p is the peak period, f is the wave frequency, while σ_w is the spectral width parameter which is given by 0.07 for $f \le f_p$ and 0.09 for $f > f_p$.

In order to model the short-crested sea state, we introduce a spreading function from DNV (Det Norske Veritas) (2021), which is defined for $|\zeta - \zeta_p| \le \frac{\pi}{2}$ as

$$X(\zeta) = \frac{\Gamma(1 + \frac{c}{2})}{\sqrt{\pi} \Gamma(0.5 + \frac{c}{2})} cos^c(\zeta - \zeta_p) \tag{7}$$

where Γ is the gamma function and ζ_p is the mean wave direction, while c is the spreading index. The spreading index is chosen as 2 which is typical for a wind-driven sea state DNV (Det Norske Veritas) (2021).

Assuming linear potential flow, we can model the free surface elevation of the short-crested sea state by means of the principle of superposition, i.e. $n \times m$ linear regular waves are superimposed,

$$\Pi(N, E, t) = \sum_{i=1}^{n} \sum_{j=1}^{m} a_{ij} \cos\left(\epsilon(N, E, t)_{ij}\right) \tag{8}$$

where $a_{ij} = \sqrt{2 S_{JS}(f_i) X(\zeta_j) \Delta f \Delta \zeta}$ is the amplitude of the ith frequency in the jth direction, whereas Δf is the frequency bandwidth and $\Delta \zeta$ is the direction bandwidth. For the sake of conciseness we have defined

$$\epsilon(N, E, t)_{ij} = \Theta_i t - k_i (N \cos(\zeta_j) + E \sin(\zeta_j)) + \mu_{ij} \tag{9}$$

where $\Theta_i = 2\pi f_i$ is the angular wave frequency, $k_i = \frac{2\pi}{L_i}$ is the wavenumber, ζ_j is the wave direction and μ_{ij} is the random phase angle for each linear wave component. For actual realization of the free surface, the wavenumbers are needed for each wave component and have to be found by iteration using an alternative form of the dispersion relation,

$$L_i = \frac{g T_i^2}{2\pi} \tanh\left(\frac{2\pi d}{L_i}\right) \tag{10}$$

where the deep water wavelength $L_i^0 = \frac{g T^2}{2\pi}$ can be used as initial guess for each wave component.

Having assumed potential flow to be applicable, the fluid particle velocities and accelerations can finally be derived from the superimposed velocity potentials associated with each wave component,

$$u_w = \sum_{i=1}^{n} \sum_{j=1}^{m} \frac{a_{i,j} g k_i}{\Theta_i} \cos(\zeta_j) \Lambda_{ij}^{\cosh} \cos(\epsilon_{ij}) \tag{11}$$

$$v_w = \sum_{i=1}^{n} \sum_{j=1}^{m} \frac{a_{i,j} g k_i}{\Theta_i} sin(\zeta_j) \Lambda_{ij}^{\cosh} \cos(\epsilon_{ij}) \tag{12}$$

$$w_w = \sum_{i=1}^{n} \sum_{j=1}^{m} -\frac{a_{i,j} g k_i}{\Theta_i} \Lambda_{ij}^{\sinh} \sin(\epsilon_{ij}) \tag{13}$$

$$\dot{u}_w \approx \sum_{i=1}^{n} \sum_{j=1}^{m} -a_{i,j} g k_i \cos(\zeta_j) \Lambda_{ij}^{\cosh} \sin(\epsilon_{ij}) \qquad (14)$$

$$\dot{v}_w \approx \sum_{i=1}^{n} \sum_{j=1}^{m} -a_{i,j} g k_i \sin(\zeta_j) \Lambda_{ij}^{\cosh} \sin(\epsilon_{ij}) \qquad (15)$$

$$\dot{w}_w \approx \sum_{i=1}^{n} \sum_{j=1}^{m} -a_{i,j} g k_i \Lambda_{ij}^{\sinh} \cos(\epsilon_{ij}) \qquad (16)$$

where $\epsilon_{ij} = \epsilon(N, E, t)_{ij}$ has been used in addition to the following definitions

$$\Lambda_{ij}^{\sinh} = \Lambda(D)_{ij}^{\sinh} = \frac{\sinh(k_i(-D+d))}{\cosh(k_i d)} \qquad (17)$$

$$\Lambda_{ij}^{\cosh} = \Lambda(D)_{ij}^{\cosh} = \frac{\cosh(k_i(-D+d))}{\cosh(k_i d)} \qquad (18)$$

which can now be used in the wave force disturbance vector in eq. (4).

4.3 Underwater current

The current effect is implemented as an additional velocity term that does not change in the water column and is transformed to be in terms of relative velocity shown in eq. (19),

$$\mathbf{M}\dot{\nu} + \mathbf{C}(\nu_r)\nu_r + \mathbf{D}(\nu_r)\nu_r + \mathbf{g}(\nu) = \tau + \tau_w \qquad (19)$$

where the relative velocity in body frame is given by $\nu_r = \nu - \nu_c$. The ocean current is given in world frame by $\mathbf{v_c}$ the body frame current velocity i found by,

$$\nu_c = \mathbf{R}^{-1}\mathbf{v_c} \qquad (20)$$

where,

$$\mathbf{v_c} = (u_c, j_c, w_c, 0, 0, 0)^\top \qquad (21)$$

u_c, j_c, w_c is the world frame water particle velocity in north, east and down direction respectably.

5. TETHER MODEL

The tether is modelled using the lumped-mass method, whereby the cable is treated as a set of $n+1$ lumped masses connected by n mass-less cylinders Hall and Goupee (2015).

Let $\mathbf{p}_{t,i} \in \mathbf{R}^3, i \in \{0, \cdots, n\}$, be the position of lumped mass i in the NED frame, and $\mathbf{v}_{t,i} = \dot{\mathbf{p}}_{t,i}$ the corresponding velocity vector. $\mathbf{p}_{t,0}$ is directly linked to the above-mentioned offshore structure which is assumed to be fixed in the world frame, $\mathbf{p}_{t,n}$ is directly attached to the ROV, hence the same position and velocity of the ROV. The dynamics associated to tether position and velocity vectors $\mathbf{p}_t$ and $\mathbf{v}_t$ can summarized as a mass-spring-damper-like system

$$\mathbf{M}_t \dot{\mathbf{v}}_t + \mathbf{D}_t \mathbf{v}_t + \mathbf{T}_i = 0 \qquad (22)$$

where $\mathbf{M}_t$ is a diagonal matrix of $n-1$ elements

$$\mathbf{M}_{t,i} = \frac{1}{2}(\mathbf{M}_{i-1} + \mathbf{M}_i + \mathbf{M}_{a,i-1} + \mathbf{M}_{a,i}) \qquad (23)$$

where $M_i \in \mathbf{R}^{3\times3}$ is the mass matrix of node i and $M_{a,i} \in \mathbf{R}^{3\times3}$ is the added mass matrix of the corresponding

cylinder. Similarly, the damping terms of diagonal matrix $\mathbf{D}_t$ are given by

$$\mathbf{D}_{t,i} = \mathbf{P}_{i-1} - \mathbf{P}_i + \mathbf{F}_i \qquad (24)$$

where $\mathbf{P}_i$, the internal damping of the tether, is expressed as

$$\mathbf{P}_i = C_t \left[(\mathbf{v}_i - \mathbf{v}_{i-1})^T \frac{\mathbf{r}_i}{|\mathbf{r}_i|} \right] \frac{\mathbf{r}_i}{|\mathbf{r}_i|} \qquad (25)$$

where C_t is a damping constant, and $\mathbf{r}_i := \mathbf{p}_{i+1} - \mathbf{p}_i$ is the vector between 2 consecutive nodes.

The tether is modelled as neutrally buoyant and the external force reduces to the hydrodynamic drag $\mathbf{F}_i$. The force $\mathbf{F}_i$ can be separated into its normal and tangential components

$$\mathbf{F}_i = \mathbf{F}_{\perp,i} + \mathbf{F}_{\|,i} \qquad (26)$$

where

$$\mathbf{F}_{\perp,i} = \frac{1}{2}\rho d_t C_\perp \mathbf{v}_{\perp,i} |\mathbf{v}_{\perp,i}| |\mathbf{r}_i| \qquad (27)$$

and

$$\mathbf{F}_{\|,i} = \frac{1}{2}\rho d_t C_\| \mathbf{v}_{\|,i} |\mathbf{v}_{\|,i}| |\mathbf{r}_i|, \qquad (28)$$

where d_t is the diameter of the tether, $\mathbf{v}_{\perp,i}$ and $\mathbf{v}_{\|,i}$ are the normal and tangential components of the flow velocity of the i-th cylinder, while $C_\perp$ and $C_\|$ are their respective drag coefficients. The normal and tangential velocity components are themselves obtained through the expressions

$$\mathbf{v}_{\perp,i} = \frac{\left[(\mathbf{v}_c - \mathbf{v}_i)^T \mathbf{r}_i \right] \mathbf{r}_i}{|\mathbf{r}_i|^2} \qquad (29)$$

(with $\mathbf{v}_c$ representing the water current velocity, expressed in the earth-fixed frame) and

$$\mathbf{v}_{\|,i} = \mathbf{v}_c - \mathbf{v}_i - \mathbf{v}_{\perp,i}. \qquad (30)$$

The term $\mathbf{k}_t$ in (22) is given by

$$\mathbf{k}_{t,i} = \mathbf{T}_i \qquad (31)$$

$\mathbf{T}_i$ is the axial tension of the i-th node is and given by

$$\mathbf{T}_i = E_t \left(\frac{A_{t,i}}{l_{0,i}} \right) \mathbf{r}_i \left(1 - \frac{l_{0,i}}{|\mathbf{r}_i|} \right), \qquad (32)$$

where $l_{0,i}$ is the length between 2 consecutive nodes at rest and l_0 is the length of the tether. The force acting on the ROV τ_t is the end node of the axial tension.

6. CONTROLLER DESCRIPTION

The controllers used in this study is based on the work done in Benzon et al. (2021), where the exact same ROV platform is used and experimentally validated for cleaning in an onshore test facility. The controller in Benzon et al. (2021) for Sway, Heave, Pitch, Roll and Yaw motion are based on SMC with an approximation on the sign function to eliminate chatter in the input; the approximation is a Sigmoid function. The controllers will be designed decoupled and the controller for the surge motion is based on SMC with integral action; see Benzon et al. (2021). The implemented controller is shown in (33).

$$\tau = \mathbf{H^{-1}}(\ddot{\mathbf{r}} - \mathbf{c_0}\dot{e} + \mathbf{b_{in}}) \qquad (33)$$

where

$$\mathbf{b_{in}}(2:6) = \rho_s \frac{\sigma}{|\sigma| + \epsilon_s} \qquad (34)$$

,

$$\mathbf{b_{in}}(1) = -k_{i,x} \cdot \sigma_x - \rho_{s,x} \frac{(S_x)}{|S_x| + \epsilon_{s,x}} \qquad (35)$$

, $\mathbf{H}$ is the input matrix, $\mathbf{r}$ is the reference, $\mathbf{e}$ is the error, $\boldsymbol{\sigma}$ is a sliding variable, S_x is an auxiliary sliding variable and $\mathbf{c_0}, \boldsymbol{\rho_s}$ and $\boldsymbol{\epsilon_s}$ are control/tuning parameters. The parameters for the controllers can be found in Benzon et al. (2021).

7. RESULTS

To quantify the cleaning performance of each test, a performance parameter, ξ, is defined based on the distance which the water jet travels to the structure, d_r, calculated as,

$$d_r = \frac{x_r}{sin(\pi - \psi)sin(\pi - \theta)} \tag{36}$$

where d_r is the distance the water jet travels before hitting the structure. x_r is the relative distance to the structure from the nozzle. As stated in Sørensen et al. (2022); Benzon et al. (2021) on a similar cleaning tool the cleaning performance is most efficient when d_r is 0.1 m, and steadily degrading until 0.2 m as the pressure is degrading, similarly the performance degrades as the nozzle gets closer to the structure as the cleaning area gets smaller. d_r will be weighted according to Fig. 2 where the weight function $W(d_r)$ is shown.
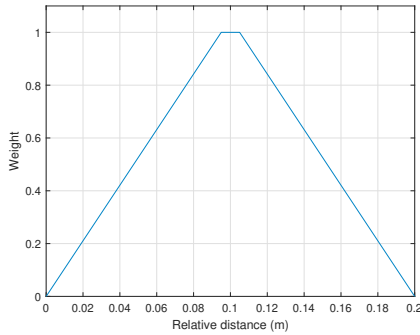
Fig. 2. Weight of relative position of nozzle to the structure.

The performance parameter can be calculate by,

$$\xi = \int W(d_r) d_r \tag{37}$$

and then normalizing it to a value between 0 and 1. A performance parameter of 0.95 is chosen as the acceptable limit. The operating conditions for the ocean waves and current will be based on data collected from an offshore structure located in the North sea. The constants used to simulate waves and current are shown in Table 5. The reference trajectory in depth and a single evaluation of the simulation results for Hs=0.2m and Hs=3m are shown in Fig. 3, this for on evaluation. 34 different evaluations is performed for each significant wave height, this is done by varying the seed of the random parameter μ, and ensures that the full spectrum is represented at each depth. The results are shown in Fig. 4-6 and is the average of 34 evaluations and represents 1530 simulations. From the results it can be seen that there is no clear effect of the ocean current in the performance parameter. This is due to the controller being able to reject the constant disturbance from the ocean current.
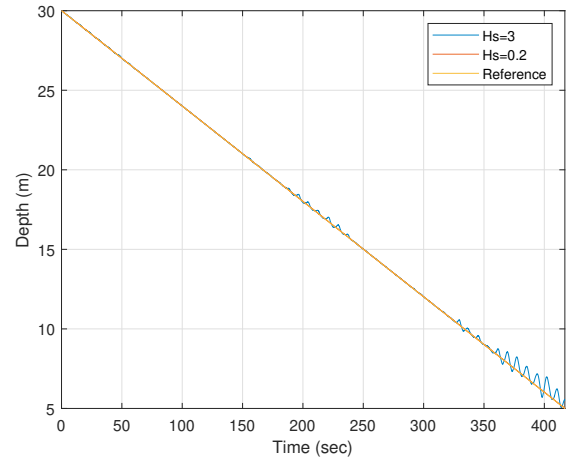
Fig. 3. Trajectory plot going from 30-5 m in depth at 0.5 ms^{-1} ocean current.

Table 5. Wave and tether constants used for simulations

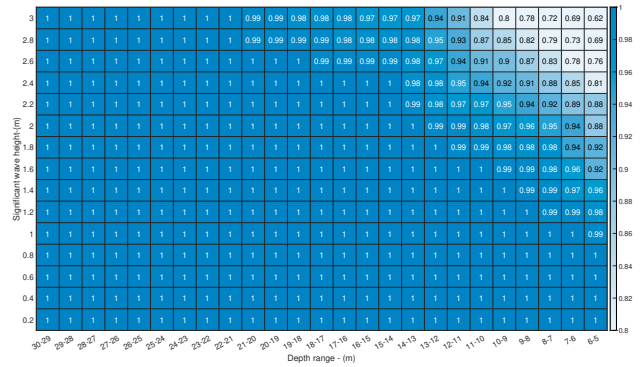| Notation	Value	Unit	Obtained from
c	2	-	DNV (Det Norske Veritas) (2021)
d	50	m	North Sea data
γ	3.3	-	JONSWAP
ζ	-0.7854	rad	North Sea data
m_{tet}	0.043	kgm^{-1}	Experimental
d_{tet}	0.0075	m	Experimental
Cn_{tet}	1.2	$-$	Souza and Maruyama (2007)
Ct_{tet}	0.01	$-$	Souza and Maruyama (2007)
C_{tet}	100	Nsm^{-1}	Souza and Maruyama (2007)
E_{tet}	$6.4 \cdot 10^{10}$	N/m^2	Souza and Maruyama (2007)
l_0	35	m	Determined

Fig. 4. Performance parameter at varying depths from 30 to 5 m and in different significant wave heights. Ocean current is constant at 0.1 ms^{-1}.

From Fig. 4-6 the performance parameter is shown at different depths with 3 different currents. Below 13 m the ROV is able to clean at all the investigated sea states and still keep a performance parameter above 0.95. Below a significant wave height of 1.4 m the ROV is able to keep a cleaning performance above 0.95 for all depths. There is a clear tendency that larger waves limits how close the ROV can get to the surface while cleaning.
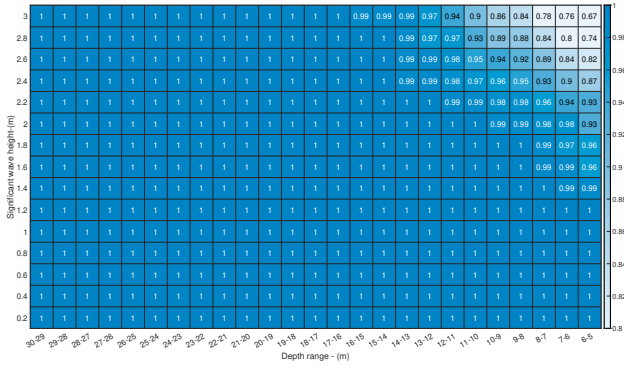
Fig. 5. Performance parameter at varying depths from 30 to 5 m and in different significant wave heights. Ocean current is constant at 0.3 ms^{-1}.
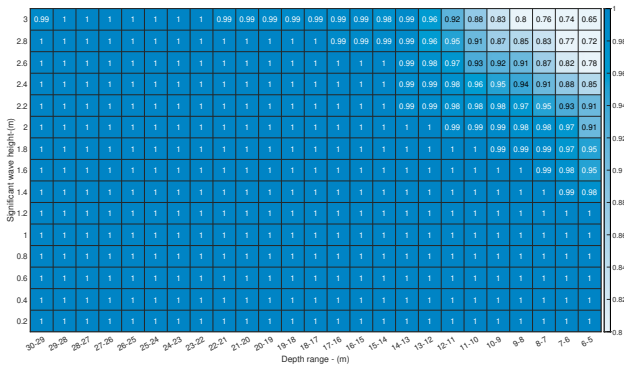

Fig. 6. Performance parameter at varying depths from 30 to 5 m and in different significant wave heights. Ocean current is constant at 0.5 ms^{-1}.

8. CONCLUSION

To conclude, this paper investigated the operating range on a validated reconfigured BlueROV2 platform used for cleaning marine growth off offshore structures in various sea states based on data gathered from the North Sea. The investigation was performed based on a simulation model which besides from a BlueROV2 model, included a model of tether based on the lumped-mass method, a model of the waves based on the JONSWAP spectrum with a spreading function to get multi-directional and irregular waves, a model of the cleaning tool and a model of the ocean current. A total of 1530 simulations were performed. To analyze the cleaning performance a normalized performance parameter was defined which weighted the relative distance of the water jet with the most efficient distance. A performance parameter of 0.95 is chosen as the acceptable limit. The results show that the waves have a larger effect on the cleaning performance compared to the ocean current. For $Hs \leq 1.4m$ it is possible to clean in the entire operating range. To clean at sea states with $Hs = 3$, the ROV needs to clean below 13 m in depth To further investigate the operating range of marine growth removing ROVs, future work should include performing the same analysis on larger more durable ROVs as the BlueROV2 has its limitation with regard cleaning offshore structures.

REFERENCES

Avila, J.P.J. and Adamowski, J.C. (2011). Experimental evaluation of the hydrodynamic coefficients of a rov through morison's equation. *Ocean engineering*, 38(17), 2162–2170. doi:10.1016/j.oceaneng.2011.09.032.

Benzon, M.S.R.v., Sørensen, F.F., Liniger, J., Pedersen, S., Klemmensen, S., and Schmidt, K. (2021). Integral sliding mode control for a marine growth removing rov with water jet disturbance. *IEEE Access.* doi:10.23919/ECC54610.2021.9655050.

DNV (Det Norske Veritas) (2021). Environmental conditions and environmental loads.

Energy Research (2020). Acomar – auto compact marine growth remover. URL https://energiforskning.dk/en/node/9795. Energiforskning.dk.

Energy Supply (2020). Ny undervandsrobot skal spare offshore-industrien for trecifret millionbeløb. URL https://www.energy-supply.dk/article/view/735752.

Fossen, T.I. (2011). *Handbook of Marine Craft Hydrodynamics and Motion Control*. Wiley, Hoboken, 1. aufl. edition.

Hall, M. and Goupee, A. (2015). Validation of a lumped-mass mooring line model with deepcwind semisubmersible model test data. *Ocean Engineering*, 104, 590–603. doi:10.1016/j.oceaneng.2015.05.035.

Hasselmann, K. (1973). *Measurements of wind-wave-growth and swell decay during the joint North Sea wave project*, volume 12. Deutsches Hydrographisches Inst, Hamburg.

Pedersen, S., Liniger, J., Sorensen, F.F., and von Benzon, M. (2022). On Marine Growth Removal on Offshore Structures. In *Proceedings of the IEEE OCEANS 2022 conference*, 1–5. Chennai.

Sayer, P. (2008). Hydrodynamic loads during the deployment of rovs. *Ocean Engineering*, 35(1), 41–46. doi:10.1016/j.oceaneng.2007.07.005.

Souza, E.C.D. and Maruyama, N. (2007). Intelligent uuvs: Some issues on rov dynamic positioning. *IEEE Transactions on Aerospace and Electronic Systems*, 43(1), 214–226. doi:10.1109/TAES.2007.357128.

Sørensen, F.F.M.v.B., Liniger, J., Pedersen, S., Klemmensen, S., and Schmidt, K. (2022). A quantitative parametric study on output time delays for autonomous underwater cleaning operations. *Journal of Marine Science and Engineering.* doi:jmse10060815.

Tena, I. (2011). Automating rov operations in aid of the oil & gas offshore industry. *SeeByte Whitepaper*, 1–9.

Yan, T. and Yan, W.X. (2003). Fouling of offshore structures in china - a review. *Biofouling (Chur, Switzerland)*, 19, 133–138. doi:10.1080/0892701021000057927.